Complementary Waveform Design with Polynomial Phase Constraint for Radar Systems

Robin Amar
SnT
University of Luxembourg
Luxembourg
robin.amar@uni.lu

Mohammad Alaee-Kerahroodi
SnT
University of Luxembourg
Luxembourg
mohammad.alaee@uni.lu

Bhavani Shankar M. R.
SnT
University of Luxembourg
Luxembourg
bhavani.shankar@uni.lu

***Abstract*—Complementary codes have been proposed to achieve ideal autocorrelation properties, which suppress sidelobes and enhance radar performance. However, the practical application of complementary sequences in radar systems is limited due to their sensitivity to Doppler shifts. These shifts introduce phase ramps, leading to slow-time mismatch and fast-time compensation challenges, which degrade the ideal sidelobe cancellation. This paper proposes a novel approach to address these limitations by incorporating a polynomial phase constraint in the design of complementary codes. The polynomial phase constraint introduces a specific phase characteristic to the sequences, improving Doppler tolerance and preserving the ideal autocorrelation properties. The optimization problem is then solved using a majorization-minimization (MM) algorithm. Simulation results demonstrate that the proposed design effectively mitigates Doppler-induced sidelobe degradation and improves radar performance, offering a promising solution for radar systems operating in dynamic environments.**

***Index Terms*—Complementary Codes, Doppler tolerance, Chirp-like sequences, Majorization-Minimization.**

I. Introduction

Waveform design plays a crucial role in modern radar systems, influencing their detection, resolution, and target identification capabilities [1]. Among the various waveform design approaches, phase coding techniques have gained significant attention due to their ability to enhance radar performance by mathematically reducing sidelobes [2]. Sidelobes pose a significant problem in radar systems, as they can lead to false detections and degrade the system's ability to resolve weak or distant targets [3]. Consequently, many studies have recently focused on designing waveforms with low sidelobe levels to improve radar performance. These studies often rely on metrics such as Peak Sidelobe Level (PSL), Integrated Sidelobe Level (ISL), Signal to Interference plus Noise Ratio (SINR), and spectral compatibility, among others [4]–[10].

One effective solution to mitigate sidelobes is the use of complementary codes [11]–[15]. Complementary codes are pairs of waveforms with ideal autocorrelation properties, which help suppress sidelobes and improve target detection. These waveforms are particularly useful in applications where the radar scene is relatively static, such as in weather radar systems, where targets like precipitation or cloud formations exhibit little motion [16]. Despite their theoretical advantages, complementary pulse pairs are not widely used due to several practical drawbacks [14]. One of the main issues is their sensitivity to Doppler shifts. Typically, the two pulses in a complementary pair are separated in time, and Doppler shift causes a phase ramp that varies as a function of time [17]. This phase ramp leads to two primary problems: (a) slow-time mismatch, where the two pulses are centered on different average phases, and (b) a phase ramp during each pulse, which requires fast-time compensation. While slow-time mismatch can be handled using conventional Doppler processing techniques that provide phase compensation over time, fast-time compensation is more challenging. Without proper fast-time compensation, the ideal delay-sidelobe cancellation is lost, leading to the appearance of near-range sidelobes. These near-range sidelobes increase with longer codes and higher Doppler shifts, further complicating the radar's performance. Additionally, (c) the signal's periodicity extends from a single pulse Repetition Interval (PRI) to multiple PRIs, thereby reducing the spacing between recurrent Doppler lobes in the ambiguity function by the same factor. Due to the aforementioned issues, the application of complementary sequences is constrained. Nevertheless, they find utility in radar-based atmospheric sensing, where target radial velocities remain relatively low [18].

In this paper, we propose a novel approach to address these challenges by designing complementary codes with a polynomial phase constraint. By introducing this constraint, we aim to mitigate the effects of Doppler shift, preserving the autocorrelation properties of complementary codes while enhancing their robustness in dynamic radar environments. This approach offers a potential solution to overcome the sensitivity issues associated with complementary pulse pairs and improve the performance of radar systems in a variety of operating conditions.

As to the background to this study, in [19] by minimizing PSL and ISL metrics, we design sequences with polynomial phase constraint for Single Input Single Output (SISO) radar systems. In [20] we extend our approach for designing sequences for Multiple Input Multiple Output (MIMO) radars, while minimizing the ISL. In this paper, we focus on designing complementary codes with the polynomial phase constraint. The polynomial phase constraint provides a new degree of freedom in the waveform design process, where, from a polynomial of degree Q, it imbibes a specific phase characteristic

in the l-th sub-sequence of the p-th transmit pulse across $\mathcal{M}_p$ pulses in a Coherent Pulse Interval (CPI). When $Q = 2$, we design chirp-like sequences, which inherently possess Doppler tolerance properties.

A. Notations

Matrices are represented by bold uppercase letters, column vectors by bold lowercase letters, and scalars by italics. The sets $\mathbb{Z}$, $\mathbb{R}$, and $\mathbb{C}$ signify the integer, real, and complex fields, respectively. The functions $\Re(\cdot)$ and $\Im(\cdot)$ extract the real and imaginary parts, respectively, and $\arg(\cdot)$ gives the phase of a complex number. The notations $(\cdot)^T$, $(\cdot)^*$, $(\cdot)^H$, and $(\cdot)^\dagger$ stand for transpose, complex conjugate, conjugate transpose, and pseudo-inverse, respectively. $\odot$ stands for hadamard product and optimal value of an optimization variable is represented as $(\cdot)^\star$. The element in the i^{th} row and j^{th} column of a matrix is denoted by $x_{i,j}$, while x_i represents the i^{th} element of the vector $\mathbf{x}$. $\mathrm{Diag}(\boldsymbol{X})$ creates a column vector containing all diagonal elements of $\boldsymbol{X}$, and $\mathrm{Diag}(\mathbf{x})$ forms a diagonal matrix, where $\mathbf{x}$ forms the principal diagonal elements of the matrix. Lastly, $\mathrm{vec}(\boldsymbol{X})$ stacks all the columns of $\boldsymbol{X}$ into a single column vector.

II. Problem Formulation

Let us consider a sequence set $\mathbf{X} = [\mathbf{x}_1, \ldots, \mathbf{x}_p, \ldots, \mathbf{x}_{\mathcal{M}_p}] \in \mathbb{C}^{N \times \mathcal{M}_p}$ with $\mathcal{M}_p$ sequences and each sequence of length N, where $\mathbf{x}_p = [x_{1,p}, \ldots, x_{N,p}]^T = [\tilde{\mathbf{x}}_{1,p}^T, \ldots, \tilde{\mathbf{x}}_{l,p}^T, \ldots, \tilde{\mathbf{x}}_{L,p}^T]^T \in \mathbb{C}^N$. A distinctive phase behavior is introduced in the l-th sub-sequence $\tilde{\mathbf{x}}_{l,p} \in \mathbb{C}^M$, of the p-th sequence by imposing a polynomial phase constraint expressed as $\arg(\tilde{\mathbf{x}}_{l,p}) = \sum_{q=0}^{Q} a_{\{q,l,p\}} m^q$, where $\arg(\mathbf{x}_{l,p}) = [\arg(x_{\{1+(l-1)M,p\}}), \ldots, \arg(x_{\{lM,p\}})]$, $a_{\{q,l,p\}}$ denotes the coefficients of the polynomial of degree q for the l-th sub-sequence in the p-th pulse. The phase variation for all the $\mathcal{M}_p$ sequences can be compactly represented as $\boldsymbol{\mathcal{A}}$, where each of its element is $a_{\{q,l,p\}}$.

We consider the Complementary Integrated Sidelobe Level (CISL) metric [21], defined as

$$\mathrm{CISL} = \sum_{k=1}^{N-1} \left| \sum_{p=1}^{\mathcal{M}_p} r_{p,p}(k) \right|^2, \tag{1}$$

where $r_{p,p}(k) = \sum_{n=1}^{N-k} x_{\{n+k,p\}} x_{n,p}^* = r_{p,p}^*(-k), p = 1, \ldots, \mathcal{M}_p$, $k = 1-N, \ldots, N-1$ and $n = 1, \ldots, N$.

Hence, the objective is to address the following optimization problem,

$$\mathcal{P} \begin{cases} \min\limits_{\boldsymbol{\mathcal{A}} \in \mathbb{R}^{Q \times L \times \mathcal{M}_p}} & \mathrm{CISL} \\ \text{subject to} & \arg(\tilde{\mathbf{x}}_{l,p}) = \sum\limits_{q=0}^{Q} a_{\{q,l,p\}} m^q, \\ & |x_{n,p}| = 1, \forall \begin{cases} n = m + (l-1)M, \\ l = 1, \ldots, L, \\ m = 1, \ldots, M, \\ p = 1, \ldots, \mathcal{M}_p. \end{cases} \end{cases} \tag{2}$$

III. Proposed Method

The objective in (2) along with the constraint ($|x_{n,p}| = 1$) after several majorization steps simplifies to an iterative optimization problem (for details refer [21]) where the i-th step involves

$$\begin{aligned} \min_{\boldsymbol{\mathcal{A}}} \quad & \| \mathbf{z} - \mathbf{y} \|_2^2, \\ \text{subject to} \quad & \arg(\tilde{\mathbf{x}}_{l,p}) = \sum_{q=0}^{Q} a_{\{q,l,p\}} m^q, \\ & |x_{n,p}| = 1, \forall \begin{cases} n = m + (l-1)M, \\ l = 1, \ldots, L, \\ m = 1, \ldots, M, \\ p = 1, \ldots, \mathcal{M}_p, \end{cases} \end{aligned} \tag{3}$$

where $\mathbf{z} = [\mathbf{x}_1^T, \mathbf{0}_{N-1}^T, \ldots \mathbf{x}_{\mathcal{M}_p}^T, \mathbf{0}_{N-1}^T]^T \in \mathbb{C}^{\mathcal{M}_p(2N-1)}$, $\mathbf{y} = ((\tilde{K}-1)\mathcal{M}_p N + \lambda_u)\mathbf{z}^{(i)} - \mathbf{R}\mathbf{z}^{(i)}$. Let $\tilde{K} = \mathcal{M}_p(2N-1)$, be the length of $\mathbf{z}$, $\mathbf{U}_k$, $\tilde{k} = 1-\tilde{K}, \ldots, \tilde{K}-1$ be $\tilde{K} \times \tilde{K}$ Toeplitz matrix, and $\mathbf{R}$ is a Hermitian Toeplitz matrix. Other additional parameters are defined in Table I. Parameters $\mathbf{f}$ and $\mathbf{r}$ can be evaluated using standard FFT/IFFT operation.

TABLE I: Additional parameters for equation (3) [20], [21].

S.No	Parameter	Expression
1	$\mathbf{F}$	$F_{n,k} = e^{-j\frac{2n\tilde{k}\pi}{2\tilde{K}}}, 0 \le n, \tilde{k} \le 2\tilde{K}$
2	$\mathbf{f}$	$\mathbf{F}[\mathbf{z}^{(i)^T}, \mathbf{0}_{1\times L}]^T$
3	$\mathbf{r}$	$\frac{1}{2L}\mathbf{F}^H\lvert\mathbf{f}\rvert^2$
4	$\mathbf{c}$	$\mathbf{r} \odot [0, \mathbf{1}_{N-1}^T, \mathbf{0}_{2(\mathcal{M}_p(2N-1)-N)+1}^T, \mathbf{1}_{N-1}^T]^T$
5	$\boldsymbol{\mu}$	$\mathbf{Fc}$,
6	λ_u	$\frac{1}{2}\left(\max\limits_{1\le\tilde{k}\le\tilde{K}} \mu_{2i} + \max\limits_{1\le\tilde{k}\le\tilde{K}} \mu_{2i-1} \right)$
7	$\mathbf{U}_k$	$\begin{cases} 1 & \text{if } j-i = \tilde{k} \\ 0 & \text{if } j-i \ne \tilde{k}, \end{cases} i,j = 1, \ldots, \tilde{K}$
8	$r_z(\tilde{k})$	$\mathbf{z}^H\mathbf{U}_{\tilde{k}}\mathbf{z}$, $\tilde{k} = 1-\tilde{K}, \ldots, \tilde{K}-1$
9	$w_{\tilde{k}}$	$\begin{cases} 1, & 1 \le \tilde{k} \le N-1 \\ 0, & N \le \tilde{k} \le \tilde{K}, \end{cases} i,j = 1, \ldots, \tilde{K}$
10	$\mathbf{R}$	$\sum_{\substack{\tilde{k}=1-\tilde{K} \\ \tilde{k}\ne 0}}^{\tilde{K}-1} w_{\tilde{k}} r_z(-\tilde{k}) \mathbf{U}_{\tilde{k}}$

As (3) is separable in the variables composing the sequence, the objective $\mathcal{O} = \| \mathbf{z} - \mathbf{y} \|_2^2$ can now be split into $\mathcal{M}_p$ subproblems and represented as

$$\begin{aligned} \mathcal{O} &= \sum_{n'=1}^{\mathcal{M}_p(2N-1)} |z_{n'} - y_{n'}|_2^2, \\ &= \sum_{n'=1}^{N} |z_{n'} - y_{n'}|_2^2 + \sum_{n'=2N}^{3N-1} |z_{n'} - y_{n'}|_2^2 \\ &\quad + \ldots + \sum_{n'=1+(\mathcal{M}_p-1)(2N-1)}^{N+(\mathcal{M}_p-1)(2N-1)} |z_{n'} - y_{n'}|_2^2 + \text{ cnst.} \end{aligned} \tag{4}$$

By omitting the terms independent of the optimization variable, the objective can be written as

$$\widetilde{\mathcal{O}} = \mathcal{O}_1 + \ldots + \mathcal{O}_p + \ldots + \mathcal{O}_{\mathcal{M}_p} = \sum_{p=1}^{\mathcal{M}_p} \mathcal{O}_p \tag{5}$$

Each of the $\mathcal{M}_p$ objectives are independent and can be solved in parallel. In (5) for brevity of expression, we consider the minimization of the p-th objective $\mathcal{O}_p$ as

$$\min_{a_{\{q,l,p\}}} \sum_{n=1+(p-1)(2N-1)}^{N+(p-1)(2N-1)} |z_n - \rho_{n,p} e^{j\psi_{n,p}}|_2^2. \tag{6}$$

The objective $\mathcal{O}_p$ for the p-th pulse is further separable in the sequence variables, therefore it is split into L parallel sub-problems corresponding to each sub-sequence as:

$$\mathcal{O}_p = \mathcal{O}_{p,1} + \ldots + \mathcal{O}_{p,l} + \ldots + \mathcal{O}_{p,L}. \tag{7}$$

Now, we introduce the constraints of Problem $\mathcal{P}$ in $\mathcal{O}_{p,l}$ directly in the entries of the sub-sequence. Hence,

$$\mathcal{O}_{p,l} = \sum_{m=1}^{M} |e^{j(\sum_{q=0}^{Q} a_{\{q,l,p\}} m^q)} - \rho_{n,p} e^{j\psi_{n,p}}|_2^2. \tag{8}$$

After simplifying the objective in (8), the reformulated problem can be represented as

$$\min_{a_{\{q,l,p\}}} -\left[\sum_{m=1}^{M} \rho_{n,p} \cos\left(\sum_{q=0}^{Q} a_{\{q,l,p\}} m^q - \psi_{n,p}\right)\right]. \tag{9}$$

Now, let $\theta_{n,p} = \sum_{q=0}^{Q} a_{\{q,l,p\}} m^q - \psi_{n,p}$. A majorizer $g(\theta_{n,p}, \theta_{n,p}^{(i)})$ of the function $f(\theta_{n,p}) = -\rho_{n,p}\cos(\theta_{n,p})$ at the i-th iteration of majorization can be obtained as

$$\begin{aligned} g(\theta_{n,p}, \theta_{n,p}^{(i)}) = &-\rho_{n,p}\cos(\theta_{n,p}^{(i)}) \\ &+ \left(\theta_{n,p} - \theta_{n,p}^{(i)}\right)\rho_{n,p}\sin(\theta_{n,p}^{(i)}) \\ &+ \frac{1}{2}\left(\theta_{n,p} - \theta_{n,p}^{(i)}\right)^2 \rho_{n,p}\cos(\theta_{n,p}^{(i)}) \end{aligned} \tag{10}$$

Employing this majorizer function, at the i-th iteration of the Majorization-Minimization (MM) algorithm, the surrogate optimization problem after converting the objective in (10) into a perfect square form can be expressed as

$$\min_{a_{\{q,l,p\}}} \sum_{m=1}^{M} \left[\rho_{n,p}\cos(\theta_{n,p}^{(i)})\left(\sum_{q=0}^{Q} a_{\{q,l,p\}} m^q\right) - b_{n,p}\right]^2 \tag{11}$$

where

$$b_{n,p} = \rho_{n,p}\cos(\theta_{n,p}^{(i)})\left(\psi_{n,p} + \theta_{n,p}^{(i)}\right) - \rho_{n,p}\sin(\theta_{n,p}^{(i)}).$$

Now, considering a generic pulse index p and l-th sub-sequence, let

$$\begin{aligned} \boldsymbol{\eta} &= [1, 2, 3, \cdots, M]^T \in \mathbb{Z}_+^M, \\ \boldsymbol{\gamma}_p &= \rho_{n,p}\cos(\theta_{n,p}^{(i)}) \odot [1, \cdots, 1]^T \in \mathbb{R}^M, \\ \mathbf{A} &= \mathrm{Diag}\,(\boldsymbol{\gamma}_p)[\boldsymbol{\eta}^0, \cdots, \boldsymbol{\eta}^Q] \in \mathbb{R}^{M\times(Q+1)}, \\ \mathbf{s} &= [a_{\{0,l,p\}}, \cdots, a_{\{Q,l,p\}}]^T \in \mathbb{R}^{Q+1}, \\ \mathbf{b} &= [b_{1,p}, \cdots, b_{M,p}]^T \in \mathbb{R}^M. \end{aligned} \tag{12}$$

In this context, $\boldsymbol{\eta}^q$ signifies that all elements of $\boldsymbol{\eta}$ are elevated to the power q individually, with q spanning from 0 to Q. By using the variables defined in (12), the optimization problem in (11) is

$$\min_{\mathbf{s}} \parallel \mathbf{A}\mathbf{s} - \mathbf{b} \parallel_2^2 \tag{13}$$

which is the standard least squares problem. The iterations are terminated with the following criterion: $\left(\frac{1}{\sqrt{NM_p}} \parallel \mathbf{X}^{(i+1)} - \mathbf{X}^{(i)} \parallel < \epsilon\right)$ where $\epsilon = 10^{-6}$. The implementation details of the proposed method are summarized in algorithm 1.

Algorithm 1 Algorithm for complimentary sequence set design with polynomial phase characteristic in every sequence

Require: $\mathcal{M}_p, N, Q, \boldsymbol{\mathcal{A}}_d^{(i)}$
$\tilde{K} = \mathcal{M}_p(2N-1)$
Set $i = 0$, initialize $\widetilde{\mathbf{X}}_d^{(0)}$
while stopping criterion is true **do**
  $\mathbf{z}^{(i)} = [\mathbf{x}_1^{(i)^T}, \mathbf{0}^T, \ldots, \mathbf{x}_{\mathcal{M}_p}^{(i)^T}, \mathbf{0}^T]^T \in \mathbb{C}^{\mathcal{M}_p(2N-1)}$
  Calculate $\mathbf{F}, \mathbf{c}, \boldsymbol{\mu}, \lambda_u$ from TABLE I
  $\mathbf{y}^{(i)} = ((\tilde{K}-1)\mathcal{M}_p N + \lambda_u)\mathbf{z}^{(i)} - \mathbf{R}\mathbf{z}^{(i)}$
  for $p \leftarrow 1$ *to* $\mathcal{M}_p$ **do**
    $\mathbf{y} = [[\tilde{\mathbf{y}}_1^T, \bar{\tilde{\mathbf{y}}}_1^T]^T, \ldots, [\tilde{\mathbf{y}}_p^T, \bar{\tilde{\mathbf{y}}}_p^T]^T, \ldots, [\tilde{\mathbf{y}}_{\mathcal{M}_p}^T, \bar{\tilde{\mathbf{y}}}_{\mathcal{M}_p}^T]^T]$
    $\widetilde{\mathbf{y}}_p^{(i)} = [\mathbf{y}_{1,p}^{T^{(i)}}, \ldots, \mathbf{y}_{l,p}^{T^{(i)}}, \ldots, \mathbf{y}_{L,p}^{T^{(i)}}]^T \in \mathbb{C}^N$
    for $l \leftarrow 1$ *to* L **do**
      $\boldsymbol{\rho} = |\mathbf{y}_{l,p}|$
      $\boldsymbol{\psi} = \arg(\mathbf{y}_{l,p})$
      $\theta_m = \sum_{q=0}^{Q} a_q m^q - \psi_m, \;\; m = 1, \ldots, M$
      $b_m = \rho_m \cos(\theta_m)\,(\psi_m + \theta_m) - \rho_m \sin(\theta_m)$
      $\boldsymbol{\eta} = [1, 2, 3, \cdots, M]^T \in \mathbb{Z}_+^M$
      $\boldsymbol{\gamma} = \rho_m \cos(\theta_m) \odot [1, \cdots, 1]^T \in \mathbb{R}^M$,
      $\mathbf{A} = \mathrm{Diag}\,(\boldsymbol{\gamma})[\boldsymbol{\eta}^0, \boldsymbol{\eta}^1, \cdots, \boldsymbol{\eta}^Q] \in \mathbb{R}^{M\times Q+1}$,
      $\mathbf{s} = [a_0, a_1, \cdots, a_Q]^T \in \mathbb{R}^{Q+1}$
      $\mathbf{b} = [b_1, b_2, \cdots, b_M]^T \in \mathbb{R}^M$
      $\mathbf{s}^\star = \mathbf{A}^{(\dagger)}\mathbf{b}$ (Least Squares Operation)
      $\tilde{\mathbf{y}}_{l,p}^{(i+1)} = \mathbf{A}\mathbf{s}^\star \in \mathbb{C}^M$
    end for
    $\widetilde{\mathbf{y}}_p^{(i+1)} = [\tilde{\mathbf{y}}_{1,p}^{T^{(i+1)}}, \ldots, \tilde{\mathbf{y}}_{l,p}^{T^{(i+1)}}, \ldots, \tilde{\mathbf{y}}_{L,p}^{T^{(i+1)}}]$
  end for
  $\mathbf{y}^{(i+1)} = [\widetilde{\mathbf{y}}_1^{T^{(i+1)}}, \bar{\widetilde{\mathbf{y}}}_1^{T^{(i+1)}}, \ldots, \widetilde{\mathbf{y}}_{\mathcal{M}_p}^{T^{(i+1)}}, \bar{\widetilde{\mathbf{y}}}_{\mathcal{M}_p}^{T^{(i+1)}}]^T$
  $x_{n,p}^{(i+1)} = e^{j\arg(y_{n,p}^{(i)})} \;\forall \begin{cases} n=1,\ldots,N, \\ p=1,\ldots,\mathcal{M}_p \end{cases}$
end while
$i \leftarrow i + 1$
return $\mathbf{X}^{(i+1)}$

IV. Simulation Results

In this section, we evaluate the performance of the proposed method and compare it with the state-of-the-art methods.

A. Waveform Characteristics

Firstly, we evaluate the convergence characteristics of Algorithm-1 using the input parameters: $N = 64$, $M = 32$, $\mathcal{M}_p = 2$ and $Q = 2$. The convergence of the objective function can be observed in Fig.1a. It demonstrates monotonic convergence throughout 10^6 iterations. The corresponding

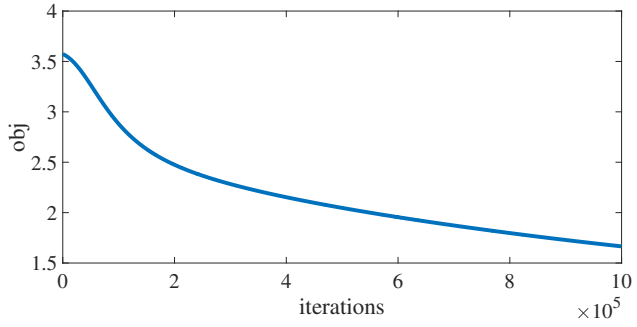

(a) Objective convergence; Algorithm-1

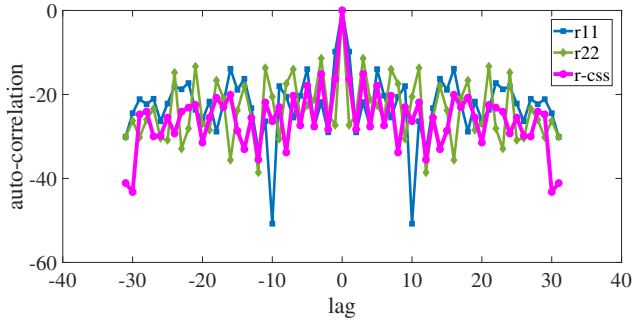

(b) CISL reduction

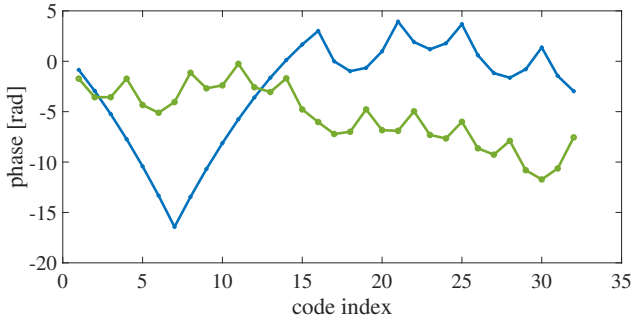

(c) Unwrapped Phase

Fig. 1: Sequence set design with quadratic phase behavior ($Q = 2$) in each sub-sequence using Algorithm-1

auto-correlation derived by coherent superposition of the auto-correlation response of each sequence in the sequence set is shown in Fig.1b (labeled: r-css). It has lower sidelobe levels due to the complementary nature of the sidelobes of each sequence. Furthermore, after applying the phase unwrap operation to every optimal sequence, a distinct quadratic phase pattern emerges within each sub-sequence, as illustrated in Fig.1c. This characteristic phase behavior contributes to the Doppler tolerance discussed in the subsequent section.

B. Doppler tolerance characteristics

The Doppler tolerance of the synthesized transmit sequence set is examined under various input conditions and assessed using the methodology outlined in [22]. For a given waveform $x(t)$, the narrowband ambiguity function S as a function of relative lag τ and Doppler shift f_D is

$$S(\tau, f_D) = \left| \int_{-\infty}^{\infty} e^{j2\pi f_D t} x(t) x^*(t+\tau) \mathrm{d}t \right|^2 \tag{14}$$

To facilitate analysis, a reference point on the ambiguity function S is selected, ensuring applicability to any constant amplitude waveform. A cross-section of the ambiguity function along the Doppler axis is extracted at the zero-delay cut, wherein the first Doppler null is designated as the reference point. This null is observed at $f_D = \pm 1/T$, where T is the pulse width. Subsequently, the maximum value of (14) across the delay axis is identified for the specified Doppler shift $f_D = \pm 1/T$. This approach guarantees that the characteristic ridge of the ambiguity function, if present, is captured while ensuring that the global peak remains unconsidered.

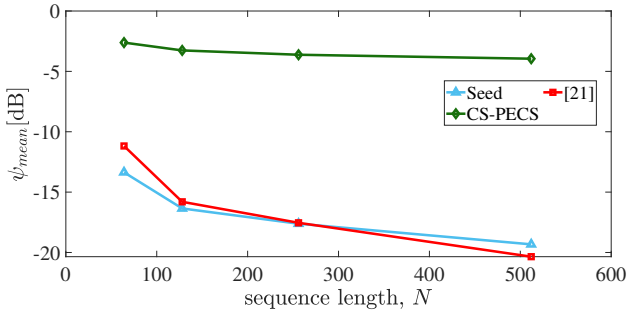

Fig. 2: Comparison of Doppler tolerance using ψ_{mean} with [21]

To quantify the Doppler tolerance of a given waveform, the metric ψ is introduced and defined as $\psi = 10\log_{10}(\eta(f_D = 1/T))$dB where

$$\eta(f_D) = \max_{\tau} \frac{S(\tau, f_D)}{S(0,0)}, \tag{15}$$

This metric provides a measure of the waveform's resilience to Doppler-induced distortions, offering insight into its suitability for applications requiring Doppler robustness.

The variation in Doppler tolerance, ψ with $Q \in [1, 2, 3, 4]$ in TABLE II is presented. The input parameters for the sequence set generation are $N = 64$, $L = 1$, and $\mathcal{M}_p = 4$. Uniquely for $Q = 2$, the mean value of ψ, $\psi_{mean} = \frac{(\sum_{i=1}^{\mathcal{M}_t} \psi_i)}{\mathcal{M}_p}$, has the highest value. Other values of Q (i.e. $Q = 1, 3$, and 4), gives rise to low values of ψ_{mean} and show high Doppler sensitivity of the sequence set.

Further, in Fig. 2, we compare the performance of the proposed method (labeled "CS-PECS") with another algorithm proposed in [21], by evaluating ψ_{mean} for each input configuration, $N = [64, 128, 256, 512]$, and $\mathcal{M}_p = 4$. Here, it is apparent that the Doppler tolerance for the proposed algorithm (with $N = M$, $L = 1$ and $Q = 2$) is the highest and outperforms the counterpart. This exhibits the significance of quadratic phase behavior in deriving Doppler tolerance characteristic.

TABLE II: Doppler tolerance variation with different values of Q for a sequence set with parameters: $N = 64$, $L = 1$, and $\mathcal{M}_p = 4$

ψ	$\mathbf{Q = 1}$	$\mathbf{Q = 2}$	$\mathbf{Q = 3}$	$\mathbf{Q = 4}$
$\mathbf{x}_1$	-9.85dB	-4.86dB	-13.11dB	-11.87dB
$\mathbf{x}_2$	-9.85dB	-3.26dB	-10.85dB	-12.36dB
$\mathbf{x}_3$	-9.85dB	-4.85dB	-15.17dB	-10.82dB
$\mathbf{x}_4$	-9.85dB	-3.15dB	-14.76dB	-11.03dB
ψ_{mean}	$\mathbf{-9.85}$dB	$\mathbf{-4.03}$dB	$\mathbf{-13.47}$dB	$\mathbf{-11.52}$dB

V. Conclusion

In this paper, we presented a mathematical approach to enhance the performance of complementary codes in radar systems by incorporating a polynomial phase constraint. This method addresses the sensitivity of complementary sequences to Doppler shifts, which typically lead to degradation in autocorrelation properties and sidelobe cancellation. By introducing a polynomial phase constraint, we were able to improve the Doppler tolerance of the complementary codes while preserving their ideal autocorrelation characteristics. The optimization problem was solved using the MM algorithm. Simulation results confirmed that the proposed design effectively mitigates Doppler-induced sidelobe degradation and offers improved radar performance in dynamic environments.

Acknowledgment

The work is supported by the Luxembourg National Research Fund (FNR) through the CORE project R4DAR under grant C23/IS/18049793/R4DAR.

References

[1] M. A. Richards, J. A. Scheer, and W. A. Holm, *Principles of Modern Radar: Basic principles*. The Institution of Engineering and Technology, 2010. [Online]. Available: https://digital-library.theiet.org/doi/abs/10.1049/SBRA021E

[2] M. Alaee-Kerahroodi, P. Babu, M. Soltanalian, and M. B. Shankar, *Signal Design for Modern Radar Systems*. Artech House, 2022.

[3] M. Alaee-Kerahroodi, A. Aubry, A. De Maio, M. M. Naghsh, and M. Modarres-Hashemi, "A coordinate-descent framework to design low PSL/ISL sequences," *IEEE Transactions on Signal Processing*, vol. 65, no. 22, pp. 5942–5956, Nov 2017.

[4] J. Song, P. Babu, and D. P. Palomar, "Optimization methods for designing sequences with low autocorrelation sidelobes," *IEEE Transactions on Signal Processing*, vol. 63, no. 15, pp. 3998–4009, 2015.

[5] L. Wu, P. Babu, and D. P. Palomar, "Cognitive radar-based sequence design via sinr maximization," *IEEE Transactions on Signal Processing*, vol. 65, no. 3, pp. 779–793, 2017.

[6] R. Jyothi, P. Babu, and M. Alaee-Kerahroodi, "SLOPE: A monotonic algorithm to design sequences with good autocorrelation properties by minimizing the peak sidelobe level," *Digital Signal Processing*, vol. 116, p. 103142, 2021.

[7] X. Feng, Y. nan Zhao, Z. quan Zhou, and Z. feng Zhao, "Waveform design with low range sidelobe and high doppler tolerance for cognitive radar," *Signal Processing*, vol. 139, pp. 143–155, 2017.

[8] S. P. Sankuru, R. Jyothi, P. Babu, and M. Alaee-Kerahroodi, "Designing sequence set with minimal peak side-lobe level for applications in high resolution radar imaging," *IEEE Open Journal of Signal Processing*, vol. 2, pp. 17–32, 2021.

[9] Q. Liu, W. Ren, K. Hou, T. Long, and A. E. Fathy, "Design of polyphase sequences with low integrated sidelobe level for radars with spectral distortion via majorization-minimization framework," *IEEE Transactions on Aerospace and Electronic Systems*, vol. 57, no. 6, pp. 4110–4126, 2021.

[10] H. Haderer, R. Feger, C. Pfeffer, and A. Stelzer, "Millimeter-wave phase-coded CW MIMO radar using zero- and low-correlation-zone sequence sets," *IEEE Transactions on Microwave Theory and Techniques*, vol. 64, no. 12, pp. 4312–4323, 2016.

[11] L. Feng, P. Fan, X. Tang, and K.-k. Loo, "Generalized pairwise Z-Complementary codes," *IEEE Signal Processing Letters*, vol. 15, pp. 377–380, 2008.

[12] C.-Y. Chen, C.-H. Wang, and C.-C. Chao, "Complete complementary codes and generalized reed-muller codes," *IEEE Communications Letters*, vol. 12, no. 11, pp. 849–851, 2008.

[13] Z. Zhang, T. Li, X. Zhang, A. Jiang, and C. Cao, "Design and analysis of complementary codes for phase coding pulse compression radar," in *2024 17th International Congress on Image and Signal Processing, BioMedical Engineering and Informatics (CISP-BMEI)*, 2024, pp. 1–5.

[14] N. Levanon, I. Cohen, and P. Itkin, "Complementary pair radar waveforms–evaluating and mitigating some drawbacks," *IEEE Aerospace and Electronic Systems Magazine*, vol. 32, no. 3, pp. 40–50, 2017.

[15] X. Liu, L. Zhao, W. Liu, J. Guo, Y. Yang, Y. Liu, and M. Peng, "Complementary coded scrambling radcom system—an integrated radar and communication design in multi-user-multi-target scenarios," *IEEE Transactions on Vehicular Technology*, vol. 73, no. 1, pp. 544–558, 2024.

[16] M. Alaee-Kerahroodi, L. Wu, E. Raei, and M. R. B. Shankar, "Joint waveform and receive filter design for pulse compression in weather radar systems," *IEEE Transactions on Radar Systems*, vol. 1, pp. 212–229, 2023.

[17] A. Pezeshki, A. R. Calderbank, W. Moran, and S. D. Howard, "Doppler resilient golay complementary waveforms," *IEEE Transactions on Information Theory*, vol. 54, no. 9, pp. 4254–4266, 2008.

[18] N. Levanon, "Noncoherent radar pulse compression based on complementary sequences," *IEEE Transactions on Aerospace and Electronic Systems*, vol. 45, no. 2, pp. 742–747, 2009.

[19] R. Amar, M. Alaee-Kerahroodi, P. Babu, and B. S. M. R., "Designing interference-immune doppler-tolerant waveforms for radar systems," *IEEE Transactions on Aerospace and Electronic Systems*, vol. 59, no. 3, pp. 2402–2421, 2023.

[20] R. Amar, M. Alaee-Kerahroodi, and B. S. M.R., "Polynomial phase constrained waveforms for mmWave MIMO radars," *IEEE Transactions on Aerospace and Electronic Systems*, pp. 1–19, 2025.

[21] J. Song, P. Babu, and D. P. Palomar, "Sequence set design with good correlation properties via majorization-minimization," *IEEE Transactions on Signal Processing*, vol. 64, no. 11, pp. 2866–2879, 2016.

[22] J. E. Quirk, R. J. Chang, J. W. Owen, S. D. Blunt, and P. M. McCormick, "A simple yet effective metric for assessing doppler tolerance," *IEEE Transactions on Radar Systems*, vol. 1, pp. 12–20, 2023.